Discrete nonlinear Schrödinger equation with defects

A. Trombettoni,[1,2] A. Smerzi,[1] and A. R. Bishop[1]
[1]*Theoretical Division and Center for Nonlinear Studies, Los Alamos National Laboratory, Los Alamos, New Mexico 87545*
[2]*Dipartimento di Fisica and Sezione INFN, Università di Perugia, Via A. Pascoli, I-06123 Perugia, Italy*
(Received 30 May 2002; published 21 January 2003)

We investigate the dynamical properties of the one-dimensional discrete nonlinear Schrödinger equation (DNLS) with periodic boundary conditions and with an arbitrary distribution of on-site defects. We study the propagation of a traveling plane wave with momentum k: the dynamics in Fourier space mainly involves two localized states with momenta $\pm k$ (corresponding to a transmitted and a reflected wave). Within a two-mode ansatz in Fourier space, the dynamics of the system maps on a nonrigid pendulum Hamiltonian. The several analytically predicted (and numerically confirmed) regimes include states with a vanishing time average of the rotational states (implying complete reflections and refocusing of the incident wave), oscillations around fixed points (corresponding to quasi-stationary states), and, above a critical value of the nonlinearity, self-trapped states (with the wave traveling almost undisturbed through the impurity). We generalize this treatment to the case of several traveling waves and time-dependent defects. The validity of the two-mode ansatz and the continuum limit of the DNLS are discussed.

DOI: 10.1103/PhysRevE.67.016607 PACS number(s): 42.25.Bs, 42.65.Tg

I. INTRODUCTION

The interplay between disorder and nonlinearity is a central topic of nonlinear science [1]. This raises a number of unsolved mathematical questions, deeply related to the behavior of many physical systems, ranging from optical fibers and waveguides [2] to polaronic materials [3], from biological molecules [4] to the dynamics of trapped dilute Bose-Einstein condensates [5]. In particular, it is highly desirable to understand how the transport properties of the nonlinear discrete media are affected by the disorder. Other important issues are related to the effect of different kinds of disorder (which can be parametric or additive, temporal or spatial), and to the modifications of the Anderson localization [6] in presence of nonlinearity.

In this paper we investigate the dynamical properties of the discrete nonlinear Schrödinger equation (DNLS) with defects, providing the details of a previously published study [5], as well as its generalization. We choose to focus on the DNLS for many reasons. First, it is a simple, highly nontrivial model where disorder, nonlinearity, and discreteness can by naturally included, and their interplay clearly singled out. Second, the continuum (translationally invariant) limit of the DNLS, the continuous nonlinear Schrödinger equation (CNLS), is a paradigm of an integrable nonlinear partial derivatives equation [7,8]. Last, but not the least, physical systems, such as Bose-Einstein condensates in deep optical lattices [9–11] and optical fibers [12–14], are described by the DNLS.

A Bose-Einstein condensate (BEC) gas can be confined in a deep optical lattice created by a far-detuned retro-reflected laser beam. In Ref. [9] a one-dimensional vertical array allowed the observation of a coherent (pulsed laser) output and of Bloch oscillations. In Ref. [11] the Bloch oscillations were created by accelerating a BEC with a frequency detuning between the two laser beams varying linearly in time. The direct observation of a Josephson atomic current in a one-dimensional array of BECs has been reported in Ref. [10]; with the coherence of multiple adjacent wells continuously probed by atomic interference.

The condensate wave function $\Psi(\vec{r},t)$ obeys in mean field the Gross-Pitaevskii equation [15]

$$i\hbar\frac{\partial\Psi}{\partial t}=-\frac{\hbar^2}{2m}\nabla^2\Psi+[V+g_0|\Psi|^2]\Psi, \tag{1}$$

where the nonlinear coupling term $g_0=4\pi\hbar^2a/m$ arises from the interatomic interaction (a is the s-wave scattering length and m is the atomic mass). The potential V can be written as the sum of the optical potential $V_{opt}(\vec{r})=V_0\cos^2[2\pi x/\lambda]$ (λ is the wavelength of the lasers and V_0 is proportional to the intensity of the laser) and of any further external potential V_{ext} superimposed to the optical array.

When V_0 is much higher than the condensate chemical potential, the system can be mapped onto the DNLS (4) [16], with ψ_n the condensate amplitude in the nth well and $\epsilon_n \propto \int d\vec{r}[(\hbar^2/2m)(\vec{\nabla}\phi_n)^2+V_{ext}\phi_n^2]$ (ϕ_n are wave functions localized in each well of the periodic potential). Then defects ϵ_n can be created with additional lasers and/or magnetic fields and can be spatially localized or extended.

A different physical system described by the DNLS is given by optical fibers: the typical experimental setup [12] is realized with an array of coupled nonlinear waveguides with similar optical properties and embedded in a different host material. The waveguides have strong nonlinear susceptibilities, whereas the host is a material with a purely linear susceptibility. When a low-intensity light is injected in one or a few neighboring waveguides, it will propagate in the array, with a spreading of its spatial distribution. The amplitude ψ_n^μ of the μth mode in the nth guide obeys the equation

$$-i\frac{\partial\psi_n^\mu}{\partial\tau}=\frac{\omega}{4p_\mu}\int dx\,dy\,\vec{E}_n^\mu\cdot\vec{P}, \tag{2}$$

where the axes of the guides are along τ, $\vec{E}_n^{\mu}$ is the electric field of μth mode in the nth guide, p_μ is the power in the μth mode, and $\vec{P}$ is the polarization [17]. For the nth guide,

$$\vec{P}/\epsilon_0 = \epsilon_H \vec{E}_n + (\epsilon_G - \epsilon_H)(\vec{E}_{n+1} + \vec{E}_{n-1}) + \chi^{(3)}(\vec{E}_n^2 + \vec{E}_{n+1}^2 + \vec{E}_{n-1}^2)\vec{E}_n, \tag{3}$$

where $\vec{E}_n$ is the total field in the nth guide, ϵ_H (ϵ_G) the dielectric coefficient of the host (guide) material, and $\chi^{(3)}$ the third-order-susceptibility, which is proportional to the Kerr coefficient. By substituting Eq. (3) in Eq. (2) and considering only the lowest single mode for each guide, we obtain the DNLS (4), with the nonlinear coefficient Λ proportional to the Kerr coefficient, and the on-site potentials ϵ_n proportional to the effective refractive indices of the individual waveguides. In the low-power limit (i.e., for small values of Λ), the optical field spreads over the whole array, while in the opposite limit the output field narrows until it localizes in a few waveguides, creating discrete solitons [12,13]. In Ref. [14] a linearly growing index was considered ($\epsilon_n \propto n$) and the Bloch oscillations have been observed. The impurities in optical fibers can be induced by different (possibly random) effective refractive indices of the guides or with varying spatial separations between them.

The plan of the paper is as follows. In Sec. II we study the propagation of an initial ''discrete'' plane wave in the presence of a single defect, and we derive the effective nonrigid pendulum Hamiltonian; we also discuss the validity of the two-mode ansatz. In Sec. III we consider an arbitrary distribution of defects and show that even in this case the dynamics maps onto a *single* nonrigid pendulum. We study in turn the cases of two defects, an extended steplike barrier, a Gaussian barrier, and a random distribution of defects. We discuss also the effect of time-dependent defects and the generalization of the two-mode ansatz to more plane waves. The continuum limit and its difference from the discrete case are also discussed. Finally, Sec. IV is devoted to the summary and to final considerations.

II. THE DISCRETE NONLINEAR SCHRÖDINGER EQUATION WITH A SINGLE DEFECT

The DNLS with defects ϵ_n in dimensionless units is

$$i\frac{\partial \psi_n}{\partial \tau} = -\frac{1}{2}(\psi_{n-1} + \psi_{n+1}) + (\epsilon_n + \Lambda|\psi_n|^2)\psi_n, \tag{4}$$

where Λ is the nonlinear coefficient and $n = 1, \ldots, N$ (N number of sites). In this section, we consider a single defect

$$\epsilon_n = \epsilon \delta_{n,\bar{n}} \tag{5}$$

at the site $\bar{n}$ and study the propagation of a plane wave $\psi(\tau = 0) = e^{ikn}$. In the following we assume $\Lambda > 0$ (which corresponds to a repulsive interatomic interaction in BECs, as is the case for ^{87}Rb atoms). However, we note that Eq. (4) is invariant with respect to the transformation $\Lambda \to -\Lambda$, $\epsilon_n \to -\epsilon_n$, and $\psi_n \to \psi_n^* e^{i\pi n}$. We will use periodic boundary conditions: thus we have $k = 2\pi l/N$ with l integer ($l = 0, \ldots, N-1$).

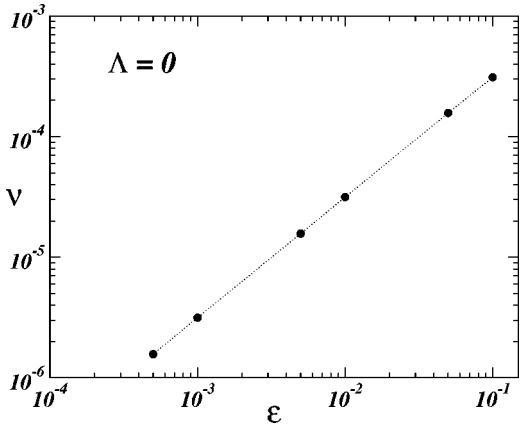

FIG. 1. Numerical (black circles) and analytical (dashed line) oscillation frequencies of the angular momentum as a function of the strength ϵ of an impurity in absence of nonlinearity; $N = 100$, $l = 10$. Note the log-log scale. The numerical analysis shows that there is no dependence of ν on the momentum $k = 2\pi l/N$.

When $\cos k < 0$ the system becomes modulationally unstable [18,19]. Stability analysis reveals that the eigenfrequencies of the linear modes become imaginary, driving an exponential growth of small perturbations. This modulation instability disappears, for $\Lambda > 0$, in the CNLS limit.

Let us consider, then, the case in which $\cos k > 0$. When $\Lambda = 0$ and the strength of the impurity is not too strong (see below), the wave is, after some finite time, coherently reflected by the defect. The angular momentum, defined as

$$L(\tau) = i\sum_n (\psi_n \psi_{n+1}^* - \text{c.c.}), \tag{6}$$

oscillates between the initial values L_0 and $-L_0$, corresponding, respectively, to plane waves with wave vector k and $-k$. This is crucially different from the continuum case where, in general, all wave vectors will enter in the dynamics (the continuum limit will be discussed in Sec. III G). We also note that the total reflection of the incident wave is the consequence of the periodic boundary conditions and the finite number of sites of the system. In an infinite chain ($N \to \infty$), the initial wave can fully or partially cross the (small) defect (depending on the strength of the nonlinearity, as in the finite system), but it will not be totally reflected.

In Fig. 1 we plot the frequency ν of the oscillations of the angular momentum; the dashed line is the result of the two-mode model (7) in which only momenta $\pm k$ enter the dynamics.

This approximation can be extended to the case of a finite nonlinearity, $\Lambda \neq 0$. In Fig. 2 we plot, as an example, the angular momentum L (normalized to the initial value L_0) for a finite value of Λ. The plot of the Fourier transforms of ψ_n at four different times is in Fig. 3: it shows that most part of

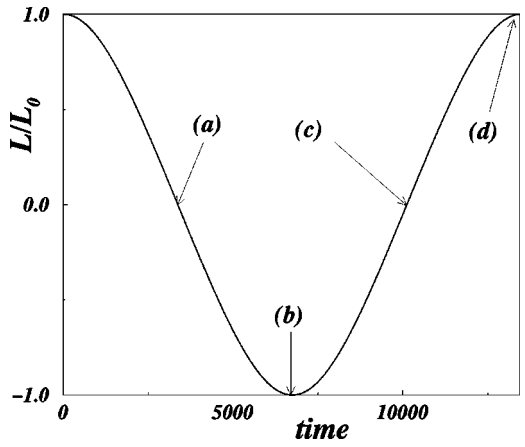

FIG. 2. Numerical (solid line) and analytical (dashed line) values of the angular momentum (normalized to the initial value L_0, vs time, with $\epsilon=0.01$, $N=40$, $l=4$, $\Lambda/\Lambda_c=0.5$, where $\Lambda_c=4\epsilon/N$. The Fourier transforms at points (a)–(d) are reported in Fig. 3.

the Fourier transform is peaked around $\pm k$. Therefore we introduce a two-mode ansatz for the dynamical evolution of the wave function:

$$\psi_n(\tau)=A(\tau)e^{ikn}+B(\tau)e^{-ikn}. \tag{7}$$

We set $A,B=\sqrt{n_{A,B}(\tau)}e^{i\phi_{A,B}(\tau)}$, $z=n_A-n_B$, and $\phi=\phi_A-\phi_B$. We will compare the numerical solution of Eq. (4) with the analytical solution of Eq. (12) obtained from ansatz (7).

Let us discuss the validity of Eq. (7). With an impurity of strength smaller than the hopping term ($\epsilon\ll 1$), the momentum distributions, peaked around $\pm k$, do not overlap. This condition preserves the two-mode dynamics through all the time scales we have been able to explore numerically. The situation changes in the (quasi)continuum limit. In this case phonons can be emitted only with quasimomentum close to k, a condition that allows the applications of the Landau superfluidity criteria (see Ref. [20] for a simple derivation of the Landau critical velocity in the CNLS). We stress, and we will show explicitly below at the end of the present section,

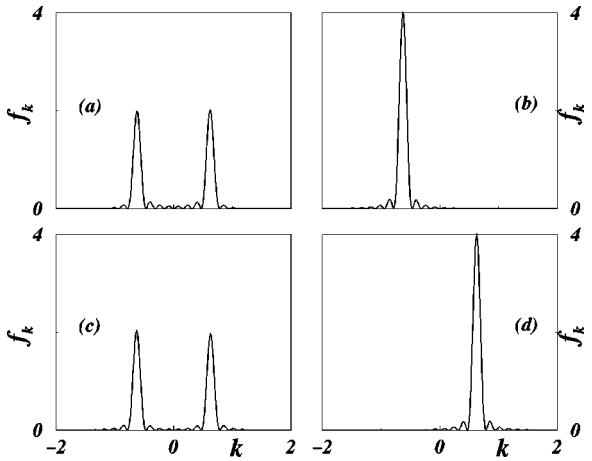

FIG. 3. Fourier transform f_k (normalized to N) of the wave function ψ_n at times marked, respectively, as (a)–(d) in Fig. 2.

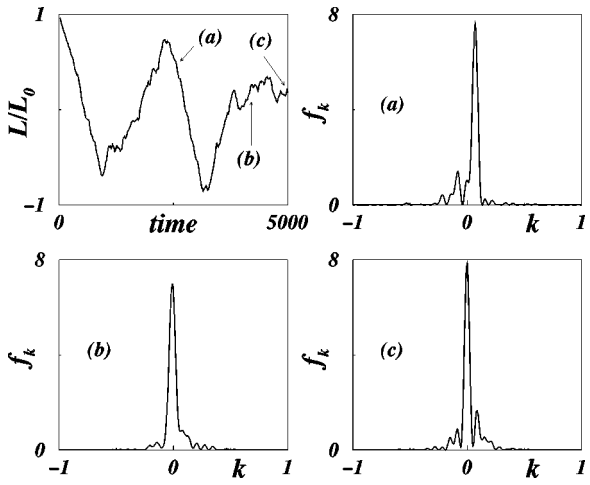

FIG. 4. Normalized angular momentum and Fourier transform f_k at times marked, respectively, as (a)–(c) in a region of parameters where the two-mode ansatz breaks down. Here $\epsilon=0.5$, $N=100$, $l=1$, and $\Lambda=2\epsilon/N$.

that the pendulum (two-mode) dynamics is crucially related to discreteness and nonlinearity, and disappears in the continuum limit. Yet, there is a striking analogy: in both cases (in the Landau and in the ''pendulum'' criteria), the phonon emission out of the incident wave (which consequently dissipates its energy) can be inhibited by an effective energy barrier. The key difference lies on the corresponding spectrum of the emitted phonons, which leads to a completely different dynamics.

To have a quantitative criterion for the validity of the two-mode ansatz (7), we observe that, in the absence of the impurities, rotational states with opposite wave vectors k, $-k$ are degenerate. The defects split the degeneracy by coupling the two $k,-k$ waves, similar to the coupling provided by the tunneling barrier in a double-well potential between the ''left'' and the ''right'' localized states. Therefore, the relative population of the two waves oscillates according to an effective generalized Josephson Hamiltonian [21]. These Josephson regimes are preserved as long as the splitting in energy induced by the defect, which is $\sim\epsilon$, is smaller than the energy gap between different rotational states. This condition can be evaluated from Hamiltonian (9): the energy of a plane wave $\psi_n=e^{ikn}$ with $k=2\pi l/N$ is $E_k=-N\cos k+N\Lambda/2$ and, putting $k'=2\pi(l+1)/N$, the minimum energy gap between different plane waves is $E_{k'}-E_k\approx 2\pi\sin k$ (for large N). Therefore we expect that the two-mode ansatz is a good approximation when $2\pi\sin k\gtrsim\epsilon$. In Fig. 4 we plot the normalized angular momentum and the Fourier transform at three different times in a case in which this condition is not satisfied, showing the failure of the two-mode ansatz. It is also obvious from the previous discussion that the two-mode dynamics will be preserved in the limit $N\to\infty$, if also $l\to\infty$ keeping $k=$const. (Note that this does not correspond to the continuous nonlinear Schrödinger equation, see Sec. III G.)

The ansatz (7) remains valid even with a time-dependent, extended, or random distribution of defects, as long as the sum of the impurity strengths remains small compared to

unity (in our dimensionless units). Furthermore, when the initial wave function is given by the sum of more waves, $\psi_n(0)=\Sigma_j A_j e^{ik_j n}$, ansatz (7) can be straightforwardly generalized as long as the quasimomentum distributions peaked around k_j do not overlap. The collision of a soliton with a single impurity has been studied, from a different perspective, in Ref. [22]. A numerical analysis of the propagation of plane waves across a segment with defects was made in Ref. [23], where a subdiffusive propagation was demonstrated, weakly depending on the nonlinearity.

Let us now come back to the derivation of the equations of motion for a single defect. We can define an effective Lagrangian as

$$\mathcal{L}=\sum_n i\dot{\psi}_n\psi_n^*-\mathcal{H}, \tag{8}$$

where the Hamiltonian of DNLS is

$$\mathcal{H}=\sum_n\left[-\frac{1}{2}(\psi_n\psi_{n+1}^*+\psi_n^*\psi_{n+1})+\epsilon_n|\psi_n|^2+\frac{\Lambda}{2}|\psi_n|^4\right] \tag{9}$$

(both $\mathcal{H}$ and the norm $\Sigma_n|\psi_n|^2=N$ are conserved). Substituting ansatz (7) in Eq. (8), we find

$$\frac{\mathcal{L}}{N}=-n_A\dot{\phi}_A-n_B\dot{\phi}_B-\Lambda n_A n_B - \frac{2\epsilon}{N}\sqrt{n_A n_B}\cos(\phi_A-\phi_B+2k\bar{n}), \tag{10}$$

where we have used the relation

$$\sum_n e^{2ikn}=0. \tag{11}$$

From Eq. (10), the Euler-Lagrange equations

$$\frac{d}{dt}\frac{\partial\mathcal{L}}{\partial\dot{q}_i}=\frac{\partial\mathcal{L}}{\partial q_i}$$

for the variational parameters $q_i(\tau)=n_{A,B},\phi_{A,B}$ give

$$\dot{z}=-\frac{2\epsilon}{N}\sqrt{1-z^2}\,\sin\phi, \tag{12a}$$

$$\dot{\phi}=\frac{2\epsilon}{N}\frac{z}{\sqrt{1-z^2}}\cos\phi+\Lambda z, \tag{12b}$$

with the replacement $\phi+2k\bar{n}\to\phi$. The total (conserved) energy is

$$H=\frac{\Lambda z^2}{2}-\frac{2\epsilon}{N}\sqrt{1-z^2}\,\cos\phi, \tag{13}$$

and the equations of motion (12) can be written in the Hamiltonian form $\dot{z}=-\partial H/\partial\phi$ and $\dot{\phi}=\partial H/\partial z$, with z and ϕ being canonically conjugate variables.

We observe that when $\Lambda=0$, Eqs. (12) give

$$\ddot{z}=-\left(\frac{2\epsilon}{N}\right)^2 z. \tag{14}$$

The oscillations of L are sinusoidal, and their frequency is given by

$$\nu=\frac{\epsilon}{\pi N}. \tag{15}$$

The comparison between numerical results and Eq. (15) is shown in Fig. 1.

Equations (12) have been studied in very different contexts, including polaron dynamics, where dimer Eqs. (12) had been solved analytically [24], and in the Josephson dynamics of two weakly coupled Bose-Einstein condensates [21]. Equations (12) are those of a nonrigid pendulum: ϕ is the angular position and z its conjugate momentum. The nonrigidity of the pendulum is due to its momentum-dependent length.

The pendulum phase portrait, z-ϕ, has been studied in detail in Ref. [25]. Let us briefly recall the main results. We have (a) oscillations around $\langle\phi\rangle=0$ and $\langle z\rangle=0$ (0 *states*); (b) oscillations around $\langle z\rangle\neq 0$ with running phase $\langle\phi\rangle\propto t$ (*self-trapped states*); (c) oscillations around $\langle z\rangle=0$ and $\langle\phi\rangle=\pi$ (π *states*); (d) oscillations about $\langle z\rangle\neq 0$ and $\langle\phi\rangle=\pi$ (*self-trapped* π *states*). The $\langle\ldots\rangle$ stands for a time average.

To understand the meaning of these regimes in our system, we observe that the angular momentum is proportional to z. Using ansatz (7) in Eq. (6), we get

$$L=2Nz\sin k. \tag{16}$$

Therefore $\langle z\rangle=0$ implies that the wave is completely reflected, and $\langle z(\tau)\rangle>0$ (or $\langle z(\tau)\rangle<0$) that the wave is only partially reflected by the impurity. The latter regime is given by a complete rotation of the pendulum about its center, and can be considered as a self-trapping of the angular momentum. Equivalently, there is an effective energy barrier that forbids the complete reflection of the incident wave and preserves its coherence. The observation of a persistent current is associated with a superfluid regime of the DNLS equation.

We can derive the critical value for the occurrence of the transition between the regimes with $\langle z\rangle=0$ (reflection of the wave) and the regimes with $\langle z\rangle\neq 0$ in the following way. Let us consider initial values $z(0)=1$ and $\phi(0)=0$: the (conserved) initial energy is $H_0=\Lambda/2$. We want to find the condition for which z cannot reach the value 0. Since $H(z=0)=-(2\epsilon/N)\cos\phi\leqslant 2\epsilon/N$, we find a critical value for the pendulum oscillations about its center given by

$$\Lambda_c=\frac{4\epsilon}{N}, \tag{17}$$

when $\Lambda<\Lambda_c$, z oscillates around 0. When $\Lambda=\Lambda_c$, asymptotically $z(\tau)\to 0$; and with $\Lambda>\Lambda_c$, $\langle z(\tau)\rangle\neq 0$. In Fig. 5 we plot the normalized angular momentum $L(\tau)/L_0$ vs time for different Λ/Λ_c in order to illustrate the transition. In Fig. 6 we plot the time average value of the normalized angular

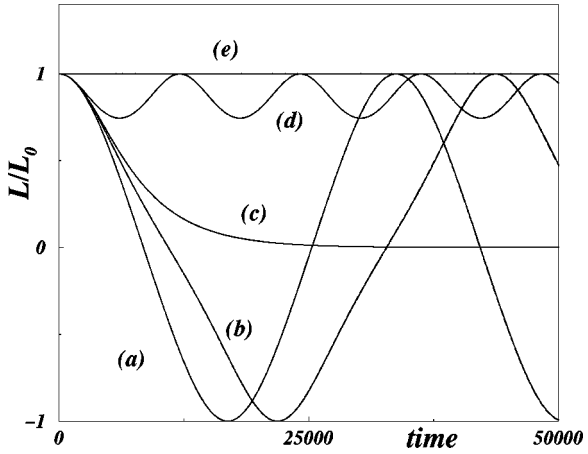

FIG. 5. Normalized angular momentum $L(\tau)/L_0$ vs time for different values of $\Lambda/\Lambda_c = 0.5, 0.75, 1, 1.5, 25$ corresponding, respectively, to points (a)–(e) $(\Lambda_c = 4\epsilon/N)$. Parameters in the simulation are $\epsilon = 0.01$, $N = 100$, $z(0) = 1$, and $\phi(0) = 0$.

momentum for different values of Λ/Λ_c and $z(0) = 1$, $\phi(0) = 0$. The numerical solutions of Eq. (4) are in agreement with the two-mode approximation (12) (dashed line). For $\Lambda < \Lambda_c$, there is, on average, no transport in the lattice.

For arbitrary initial conditions, the critical value of Λ is given by

$$H[\phi(0), z(0)] = 2\epsilon/N. \tag{18}$$

As a further difference from the Landau criteria, we remark that the critical value for self-trapping (and superfluidity) in the case of a single impurity does depend on the strength of the defect, but not on the quasimomentum k.

Let us now study the fixed points of Eqs. (12) and the related physical regimes. By solving for $\dot{z} = 0$, $\dot{\phi} = 0$, we find first

$$z = 0, \tag{19a}$$

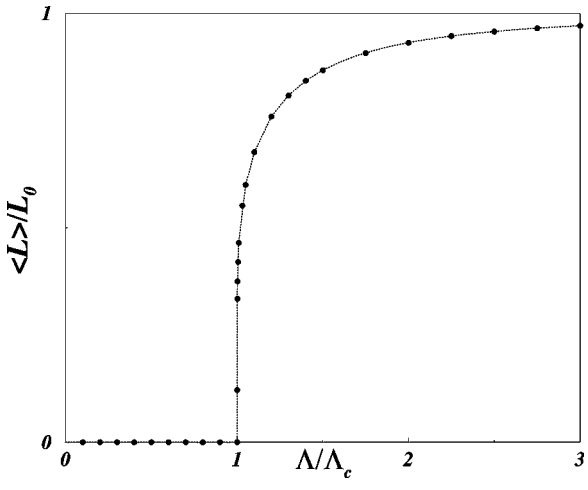

FIG. 6. Average value of the normalized angular momentum vs the nonlinear coefficient Λ/Λ_c. The filled circles are the numerical solutions of Eq. (4); the dashed line is obtained from Eqs. (12). Parameters are the same as in Fig. 5.

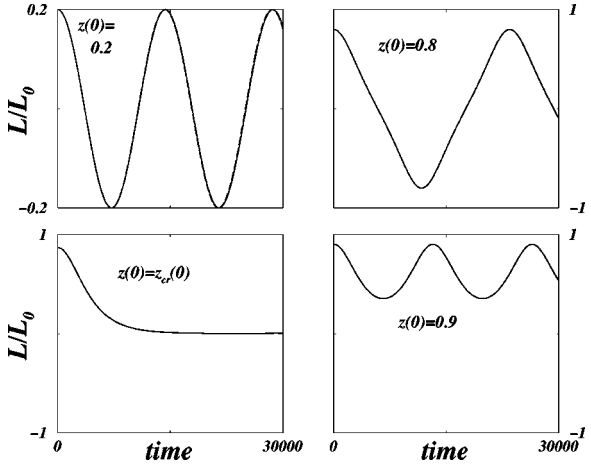

FIG. 7. Normalized angular momentum as a function of time for $\Lambda = 8\epsilon/N$, $\phi(0) = 0$, and different values of $z(0)$. From Eq. (20), $z_{cr}(0) = \sqrt{3/4}$. Solid line: numerical results; dashed line: analytical model. In the numerical simulations, $\epsilon = 0.01$, $N = 100$, and $l = 10$.

$$\phi = 2m\pi, \tag{19b}$$

with $|A| = |B|$ (m is an integer). This corresponds to a time-independent solution $\psi_n \propto \cos(kn)$ and to a minimum of energy (13). The fixed point (19) is stable and the oscillations about it are the 0 states: the small-amplitude oscillations have frequency $\propto \sqrt{1+\Lambda}$. In Fig. 7 we show the large-amplitude oscillations, comparing numerical and analytical solutions: we fix Λ and $\phi(0) = 0$, and vary the initial imbalance $z(0)$. By using the same argument as before, when $z(0)$ is smaller than a critical value $z_{cr}(0)$, we have $\langle z(0) \rangle = 0$. By approaching $z_{cr}(0)$, the oscillations become more and more anharmonic, and they go to 0 asymptotically for $z_{cr}(0)$. For $z(0) > z_{cr}(0)$, the self-trapped regime is retrieved. By using Eq. (18), we find

$$z_{cr}^2(0) = \frac{2\left(\dfrac{\Lambda}{4\epsilon/N}\right) - 1}{\left(\dfrac{\Lambda}{4\epsilon/N}\right)^2}. \tag{20}$$

The other fixed points of Eqs. (12) are

$$z = 0, \tag{21a}$$

$$\phi = (2m+1)\pi, \tag{21b}$$

and

$$z = \pm\sqrt{1 - \frac{2\epsilon/N}{\Lambda}}, \tag{22a}$$

$$\phi = (2m+1)\pi. \tag{22b}$$

The fixed point (21) corresponds to a time-independent solution of Eq. (4) of the form $\psi_n \propto \sin(kn)$, and the oscillations around it are the π states previously introduced. The oscil-

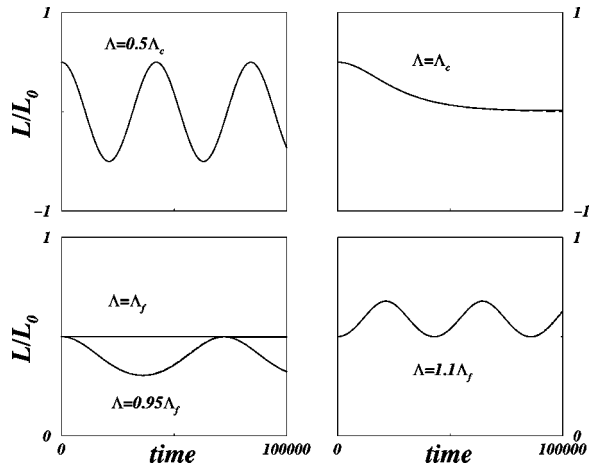

FIG. 8. Normalized angular momentum as a function of time for $\Lambda<\Lambda_c$, $\Lambda=\Lambda_c$, $\Lambda<\Lambda_f$, $\Lambda=\Lambda_f$, $\Lambda>\Lambda_f$. Λ_c and Λ_f are given, respectively, by Eqs. (23) and (24). Solid line: numerical results; dashed line: analytical model. In the numerical simulations, $\epsilon=0.01$, $N=100$, $l=10$, $\phi(0)=\pi$, and $z(0)=0.5$.

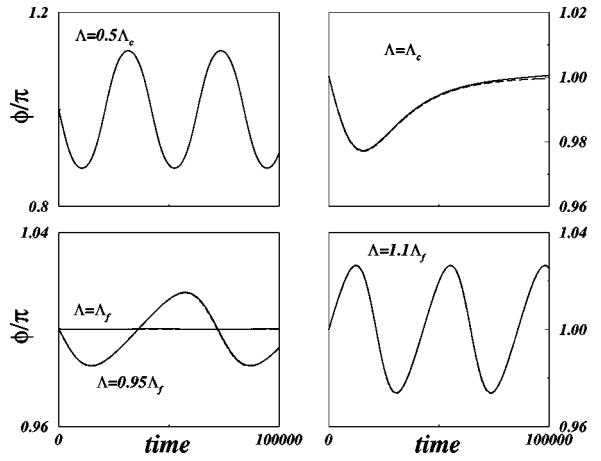

FIG. 9. Phase vs time for the cases of Fig. 8.

lations around Eq. (22) are the self-trapped π states, in which the nonrigid pendulum completes oscillations on its inverted state.

Let us fix $z(0)$ and $\phi(0)=\pi$, and vary Λ. By using Eq. (18), we find the following critical value for the nonlinearity:

$$\Lambda_c=\frac{4\epsilon[1-\sqrt{1-z^2(0)}]}{Nz^2(0)}. \tag{23}$$

When $\Lambda<\Lambda_c$, z oscillates around 0 and ϕ around π. For $\Lambda=\Lambda_c$, z asymptotically reaches 0, and ϕ reaches π. Above Λ_c, we have oscillations around a nonzero value: this means that we are in a superfluid regime with the plane wave passing through the defects. In this region of parameters, the phase difference between the transmitted wave and the reflected one is, on average, equal to π. This system can be therefore used to tune this phase difference. There are effectively two kinds of these self-trapped π states, and they are separated by the value Λ_f corresponding to the fixed point (22). We find

$$\Lambda_f=\frac{2\epsilon/N}{\sqrt{1-z^2(0)}}. \tag{24}$$

When $\Lambda<\Lambda_f$, z oscillates around a value smaller than $z(0)$. When $\Lambda=\Lambda_f$, we are at the fixed point $z(t)=z(0)$. When $\Lambda>\Lambda_f$, z oscillates around a value greater than $z(0)$. In all these three cases, the average value of ϕ is π. We remark that

$$\frac{\Lambda_f}{\Lambda_c}=\frac{z^2(0)}{2\sqrt{1-z^2(0)}[1-\sqrt{1-z^2(0)}]},$$

and therefore, since z cannot exceed 1, is always $\Lambda_f>\Lambda_c$.

In Figs. 8 and 9 we plot the angular momentum and the phase ϕ for $\Lambda<\Lambda_c$ (where $\langle z\rangle=0$), $\Lambda=\Lambda_c$ (where for large times $\langle z\rangle\to 0$), $\Lambda_c<\Lambda<\Lambda_f$ [where $\langle z\rangle<z(0)$], $\Lambda=\Lambda_f$ [where $z(t)=z(0)$], and $\Lambda<\Lambda_f$ [where $\langle z\rangle>z(0)$]. In all the cases, $\langle\phi\rangle=\pi$, and the numerical solutions of Eq. (4) are compared with our analytical model.

III. ARBITRARY DISTRIBUTION OF DEFECTS

The previous discussion can be generalized to the case of many impurities. The effective Hamiltonian (13) becomes $H=(\Lambda z^2/2)-(2/N)\sqrt{1-z^2}\Sigma_n\epsilon_n\cos(\phi+2kn)$, which can be written as a simple, single nonrigid pendulum Hamiltonian:

$$H=\frac{\Lambda z^2}{2}-\frac{2\overline{\epsilon}}{N}\sqrt{1-z^2}\cos(\phi+\alpha), \tag{25}$$

with $\overline{\epsilon}$ and α given by the Fourier transform of the defect distribution:

$$\overline{\epsilon}e^{i\alpha}=\sum_n \epsilon_n e^{2ikn}. \tag{26}$$

Equations (25) and (26) are the main results of this paper. The critical value Λ_c is given by Eq. (18), with the replacement

$$\epsilon\to\overline{\epsilon};\phi(0)\to\phi(0)+\alpha. \tag{27}$$

Below, we consider applications of these results to several specific defect forms.

A. Two defects

Let us consider, first, the case of two isolated impurities:

$$\epsilon_n=\epsilon_1\delta_{n,\overline{n_1}}+\epsilon_2\delta_{n,\overline{n_2}}. \tag{28}$$

From Hamiltonian (25), we find the equations of motion for z and ϕ, which we write in the form (with the replacement $\phi+2k\overline{n_1}\to\phi$):

$$\dot{z}=-\frac{2\epsilon_1}{N}\sqrt{1-z^2}\sin\phi-\frac{2\epsilon_2}{N}\sqrt{1-z^2}\sin(\phi+\Delta\phi_{12}), \tag{29a}$$

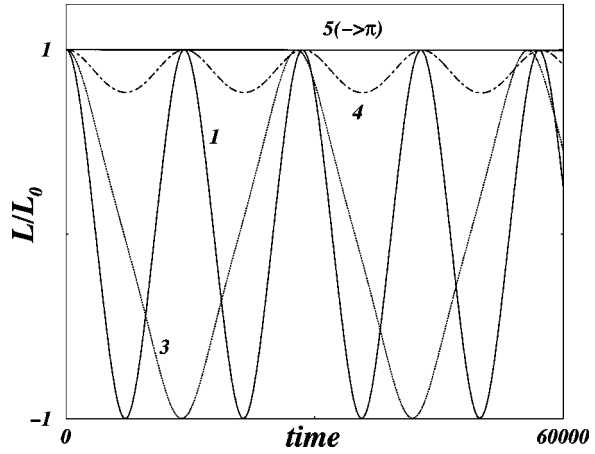

FIG. 10. Normalized angular momentum vs time for different distances of two equal impurities. The different distances are 1, 3, 4, and 5 sites. Since $\Delta\phi_{12}=(\bar{n}_2-\bar{n}_1)\pi/5$, when the distance is 5 sites, the corresponding critical value for the transition is $\Lambda_c(\Delta\phi_{12}=\pi)=0$ and the system is not transparent to the impurities. When the distance is 10 sites, $\Lambda(\Delta\phi_{12}=2\pi)=8\epsilon/N$. The critical value for different $\Delta\phi_{12}$ is given by Eq. (31), and determines the transmission or nontransmission of the wave. Parameter values: $\epsilon_1=\epsilon_2=0.005$, $N=40$, $l=2$, $\Lambda/\Lambda_c(\Delta\phi_{12}=2\pi)=0.5$, $z(0)=1$, and $\phi(0)=0$.

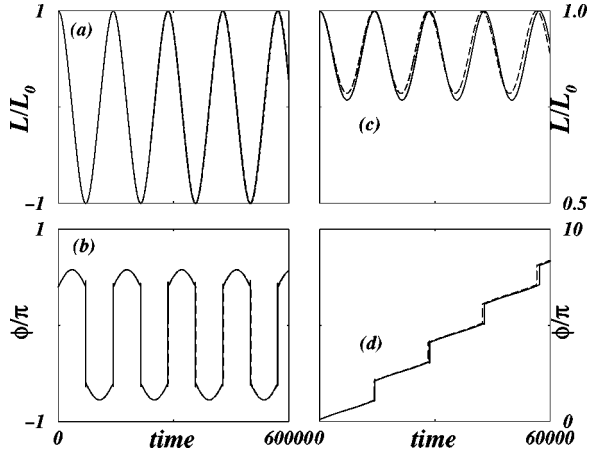

FIG. 11. Normalized angular momentum *(a)* and phase *(b)* vs time for distances 1 and 11 sites: $\Delta\phi_{12}$ differs by 2π and the numerical results are almost equal, as explained in the text. The solid line corresponds to the numerical solution, and the dashed line to the solution of Eqs. (29). In *(c)* and *(d)*, we plot L/L_0 and ϕ/π for distances of 4 and 14. Since the critical value of Λ_c is decreased, as predicted by Eq. (18), we obtain a self-trapped solution, unlike *(a)* and *(b)* where the same values are used with a different distance between the impurities. Parameter values in the simulations: $\epsilon_1=\epsilon_2=0.005$, $N=40$, $l=2$, $\Lambda/\Lambda_c(\Delta\phi_{12}=2\pi)=0.5$, $z(0)=1$, and $\phi(0)=0$.

$$\dot{\phi}=\Lambda z+\frac{2\epsilon_1}{N}\frac{z}{\sqrt{1-z^2}}\cos\phi+\frac{2\epsilon_2}{N}\frac{z}{\sqrt{1-z^2}}\cos(\phi+\Delta\phi_{12}), \tag{29b}$$

where $\Delta\phi_{12}=2k(\bar{n}_2-\bar{n}_1)$. $\bar{\epsilon}$ and α of Eq. (26) are expressed in terms of ϵ_1, ϵ_2, and $\Delta\phi_{12}$ by the relations $\bar{\epsilon}=\sqrt{\epsilon_1^2+\epsilon_2^2+2\epsilon_1\epsilon_2\cos\Delta\phi_{12}}$, and $\tan\alpha=\epsilon_2\sin\Delta\phi_{12}/(\epsilon_1+\epsilon_2\cos\Delta\phi_{12})$. The effective Hamiltonian is

$$H=\frac{\Lambda z^2}{2}-\frac{2\epsilon_1}{N}\sqrt{1-z^2}\cos\phi-\frac{2\epsilon_2}{N}\sqrt{1-z^2}\cos(\phi+\Delta\phi_{12}). \tag{30}$$

We see that the spatial distance between the two impurities enter in the dynamics only through the relative phase $\Delta\phi_{12}$ $(\mathrm{mod}\,2\pi)$. Now the critical value Λ_c, and therefore the transparency of the system to the impurities, depends on this phase difference.

In the case $\epsilon_1=\epsilon_2\equiv\epsilon$, it is easily seen that when $\Delta\phi_{12}=\pi$, the system is not transparent to the impurities and the plane wave is always transmitted. Similarly, when $\Delta\phi_{12}=2\pi$, the effective defect is given by $\epsilon_{eff}=2\epsilon$. In Fig. 10, we consider the case of two equal impurities: we choose $N=40$ sites and $l=2$, so that $2k=\pi/5$ and $\Delta\phi_{12}=(\bar{n}_2-\bar{n}_1)\pi/5$. When the distance between the two impurities is 5 sites, then $\Delta\phi_{12}=\pi$, and we have transparency to the impurities. This can be numerically seen by fixing $z(0)$, $\phi(0)$, and Λ, and varying the distance between the impurities. In Fig. 11 we plot the dynamical evolution of the angular momentum and phase for two different distances of the impurities: the numerical solutions are compared with the solution of Eqs. (29).

The critical value Λ_c is determined in the following way. Let us suppose for simplicity that $z(0)=1$ and $\phi(0)=0$: the conserved energy is $H(0)=\Lambda/2$. In the instant at which $z=0$, it is $H(z=0)\equiv h(\phi)/N$, where $h(\phi)=-2\epsilon[\cos\phi+\cos(\phi+\Delta\phi_{12})]$. The function h has a maximum in ϕ_{max}, which is given by

$$\tan\phi_{max}=-\sin\Delta\phi_{12}/(1+\cos\Delta\phi_{12}),$$

the critical value for which z asymptotically reaches 0 is given by

$$\Lambda_c=\frac{2}{N}h(\phi_{max}). \tag{31}$$

We have a similar formula for the general case $\epsilon_1\neq\epsilon_2$. In Fig. 12, we plot Λ_c vs $\Delta\phi_{12}$ by choosing $2k=\pi/5$ (i.e., $\Delta\phi_{12}=\pi/5$ when the two impurities are in the neighbor sites) and show the comparison between the numerical values and Eq. (31): the system is transparent (i.e., $\Lambda_c=0$, which means that the wave always passes) when $\Delta\phi_{12}=2\pi$, as the two-mode result [Eq. (30)] predicts.

B. Step barrier

We now consider an extended, steplike barrier: $\epsilon_n=\mathrm{const}$ for $\bar{n}_1\leqslant n\leqslant\bar{n}_2$. Similar to the case of two isolated impurities, we can choose the length of the step in such a way that the system is not transparent to the defects: e.g., with $2k=\pi/5$, when the length of the barrier is 10 sites, Eq. (26) vanishes and the system becomes transparent. This is illustrated in Fig. 13, where we consider the same initial conditions [$z(0)=1$ and $\phi(0)$] and different lengths L of the

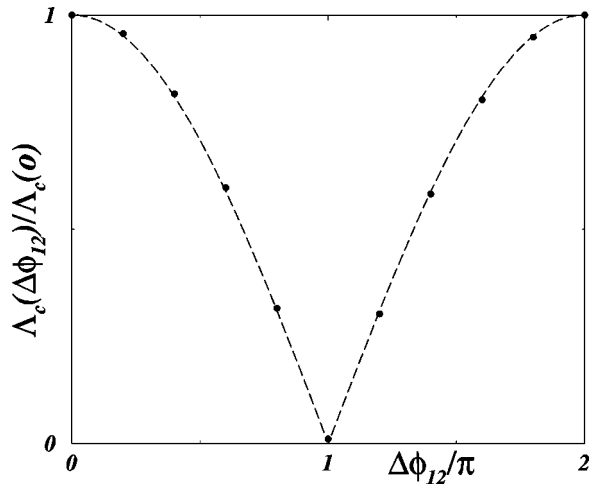

FIG. 12. Plot of the critical value Λ_c vs the phase difference $\Delta\phi_{12}$ associated with two equal impurities $\epsilon_1=\epsilon_2\equiv\epsilon$. Numerical simulations (solid points) are with $N=40$ and $l=2$, so $\Delta\phi_{12}=\Delta n\pi/5$ with Δn the distance between the two impurities. The dashed line is Eq. (31), $\epsilon=0.005$, $z(0)=1$, $\phi(0)=0$. In the plot, Λ is normalized to the critical value $\Lambda_c(\Delta\phi_{12}=0)$, i.e., with $\Delta\phi_{12}$ being a multiple of 2π.

step: when this changes from 1 to 10, the system displays the ''pendulum'' transition to superfluidity.

C. Gaussian barrier

Here we consider a Gaussian barrier with width σ centered on the site $\bar{n}$:

$$\epsilon_n=\frac{\epsilon}{\sqrt{\pi}\sigma}e^{-(n-\bar{n})^2/\sigma^2}. \tag{32}$$

We choose the coefficient in order that by changing the sum to integrals, which is correct for large N and for $\sigma\gtrsim 1$ [26],

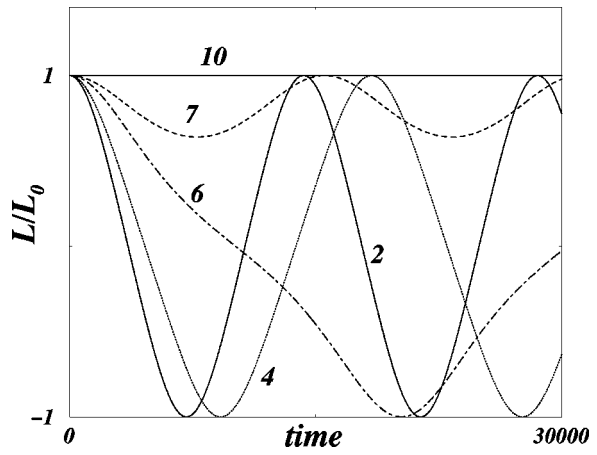

FIG. 13. Plot of the normalized angular momentum vs time for different lengths L of the step: $\epsilon_n=$const for $\bar{n}\leq n\leq\bar{n}+L-1$. We consider $L=2$, 4, 6, 7, and 10 sites. Parameter values: $N=40$, $l=2$, $z(0)=1$, and $\phi(0)=0$. Λ is chosen to be $2\epsilon/N$, where $\epsilon=0.01$ is the sum of the impurities. Since $2k=\pi/5$, when the length of the barrier is 10, the system is transparent to the impurities.

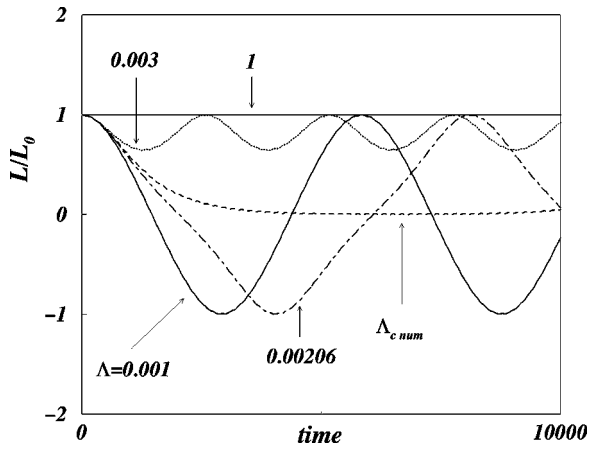

FIG. 14. Angular momentum vs time for different values of Λ in the case of a Gaussian barrier with width $\sigma=3$ and normalized to $\epsilon=0.05$. The numerical critical value is 0.002 28, and the value obtained from Eq. (35) is 0.002 06. Parameter values in the simulations: $N=40$, $l=2$, $z(0)=1$, and $\phi(0)=0$.

we have $\Sigma_n\epsilon_n\approx\int dn\,\epsilon_n=\epsilon$. As we discussed in Sec. II, the two-mode ansatz (7) works if ϵ is much smaller than the hopping term. Substituting sums with integrals everywhere, by using Eq. (31), we get

$$H\approx\frac{\Lambda z^2}{2}-\frac{2\epsilon e^{-k^2\sigma^2}}{N}\sqrt{1-z^2}\cos(\phi+2k\bar{n}). \tag{33}$$

This means that the effect of an extended barrier is equal to that of a single impurity with effective strength

$$\epsilon_{eff}=\epsilon e^{-k^2\sigma^2}. \tag{34}$$

For example, with initial values $z(0)=1$ and $\phi(0)=0$, the critical value obtained from Eq. (17) is

$$\Lambda_c=\frac{4\epsilon_{eff}}{N}. \tag{35}$$

In Fig. 14 we plot the normalized angular momentum for different values of Λ: the critical value is in reasonable agreement with Eq. (35), and the agreement improves by increasing the number of sites in the lattice.

It is important to remark that in the present case the critical value depends on the momentum of the incident plane wave: when $k\sigma\gg 1$, then $\Lambda_c\to 0$. This means that a plane wave with large momentum will always pass through the barrier, as expected. In Fig. 15, we compare the critical value Λ_c, numerically found for different wave vectors k, with the analytical prediction (35).

D. Random distribution of defects

We now consider the case of uniformly distributed random defects. All the regimes discussed so far have been found to be in agreement with full numerical analysis also in this case.

From Eq. (26) we see that distributions of defects with different means, but equal values of $\bar{\epsilon}$ and α, have the same

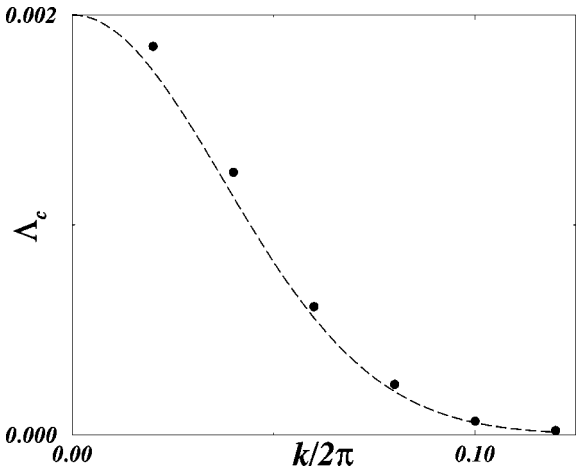

FIG. 15. Critical value of Λ as a function of the wave vector k of the incident plane wave. Black circles are numerical results; dashed line from Eq. (35). Parameter values in the simulations: $N=100$, $z(0)=1$, and $\phi(0)=0$. The width of the barrier is $\sigma=3$ and the sum of the impurities is 0.05.

threshold for the occurrence of the superfluid regime. When $\phi(0)=0$, the critical value is given by

$$\Lambda_c=\frac{4\bar{\epsilon}}{N}, \tag{36}$$

so it depends only on $\bar{\epsilon}$. This is explicitly shown in Fig. 16, in which we compare Λ_c from Eq. (36) with the numerical results obtained using a distribution with all the $\epsilon_n>0$, or all the $\epsilon_n<0$, or with zero mean value. In Fig. 17, we plot L/L_0 as a function of time for various Λ and a random distribution of defects ϵ_n. The critical value Λ_c calculated from Eq. (36), as well as the oscillation profiles, are compared with the numerical findings.

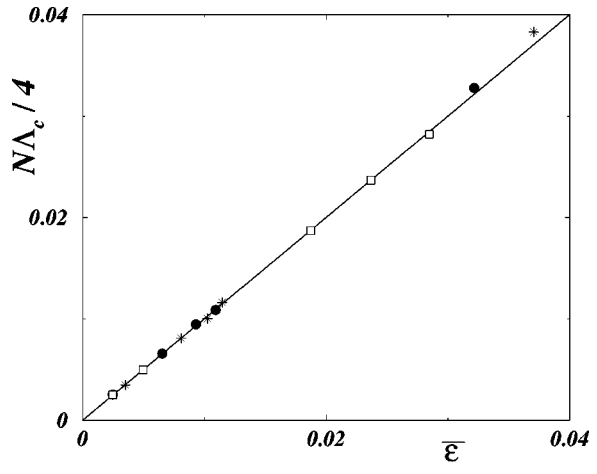

FIG. 16. Critical value Λ_c vs $\bar{\epsilon}$ for different random distributions of defects [and initial values $z(0)=1$ and $\phi(0)=0$]. The solid line is the analytical prediction (36), the black circles are the filled squares, and the stars correspond to the numerical solutions of the DNLS (4) with an uniform distribution of the random defects having, respectively, positive, negative, and zero mean values.

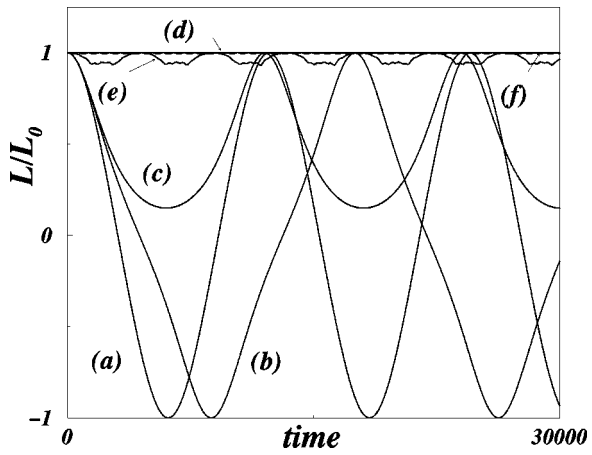

FIG. 17. Angular momentum vs time with a random distribution of defects for different values of $\Lambda/\Lambda_c=0.45$, 0.90, 1.01, 10,100, and 1000 (corresponding to $a-f$), $z(0)=1$, and $\phi(0)=0$. The sum of the strengths of the random impurities is 0.1, and the critical value Λ_c is given by Eq. (31).

E. Time-dependent defects

We discuss how to generalize ansatz (7) in the case of a time-dependent defect. First, we consider a single time-dependent defect at site $\bar{n}$, choosing as an example an oscillatory driving:

$$\epsilon_n=\epsilon\cos(\omega t)\,\delta_{n,\bar{n}}. \tag{37}$$

The effective Hamiltonian (13) becomes

$$H=\frac{\Lambda z^2}{2}-\frac{2\epsilon\cos(\omega t)}{N}\sqrt{1-z^2}\cos\phi, \tag{38}$$

and it describes a nonrigid pendulum with a time-dependent length. Our aim, in the present paper, is not to investigate the DNLS with such a time-dependent external drive, but rather to show that the two-mode ansatz (7) and the mapping on the effective Hamiltonian (38) still give a quantitative account for the dynamics of the system, leaving a systematic study for further investigations. In Fig. 18, we compare, for four different values of ω, the normalized angular momentum obtained from the numerical solution of the DNLS with the defect (37), with the results of the analytical model.

F. Generalization of the two-mode ansatz

We now discuss the case in which we have two plane waves with initial momenta k_1 and k_1. If k_1 and k_2 are not too close (i.e., if the Fourier transforms do not overlap), the numerical study of the solutions of the DNLS shows that during the dynamics only the wave vectors $\pm k_1$ and $\pm k_2$ play a role. In Fig. 19, we show an example of the Fourier transform at different times. Therefore we can write the wave function as

$$\psi_n(\tau)=A(\tau)e^{ik_1 n}+B(\tau)e^{-ik_1 n}+C(\tau)e^{ik_2 n}+D(\tau)e^{-ik_2 n}. \tag{39}$$

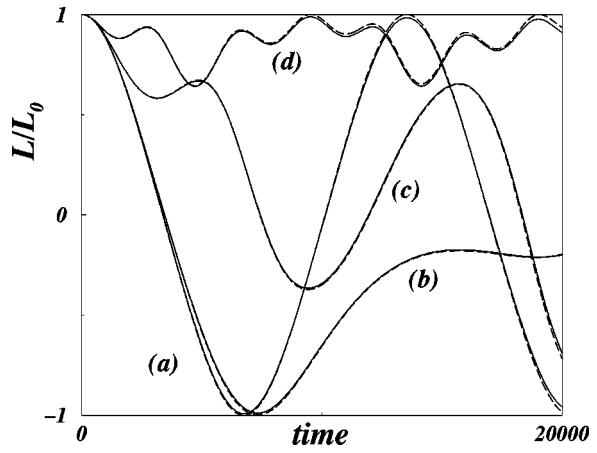

FIG. 18. Normalized angular momentum vs time for a defect $\epsilon_n=\epsilon\cos(\omega t)$, and $\omega/\Lambda_c=0.01$, 0.1, 0.5, and 1 (with $\Lambda_c=4\epsilon/N$) corresponding, respectively, to cases (a)–(d). Solid line is numerical solution; dashed line from analytical model. Parameters: $\epsilon=0.01$, $N=40$, $l=4$, and $\Lambda/\Lambda_c=0.5$.

A similar situation occurs if the initial condition is given by a discrete Gaussian, whose Fourier transform is very localized (say around k_c). In this case, ansatz (39), which in momentum space is $f_k=A(\tau)\delta(k_1-k)+B(\tau)\delta(k_1+k)+C(\tau)\delta(k_2-k)+D(\tau)\delta(k_2+k)$ (where f_k is the Fourier transform of ψ_n), becomes

$$f_k(\tau)=A(\tau)g_A(k-k_c)+B(\tau)g_B(k+k_c), \tag{40}$$

where g_A and g_B are the Gaussians, with widths σ_A and σ_B to be determined variationally (together with A and B). We will present the result of such a study in a separate paper.

G. The continuum limit

In the CNLS, which can be considered as a translationally invariant limit of the DNLS, an argument due to Landau (see Ref. [20]) implies that a nonlinearity allows a superfluid propagation of a wave with velocity smaller than the sound velocity (for weak perturbations). A simple derivation of the Landau critical velocity in the CNLS was recently proposed in Ref. [20], considering an annular geometry with a single (small) impurity. Also in this case it is possible to map the problem of the propagation of a plane wave to a Josephson-like Hamiltonian. The key point is that the nonlinearity provides an effective energy barrier against the creation of elementary excitations with momenta $k+q,k-q$ (with q arbitrarily small), which would dissipate the energy of the incident wave having momentum k. This scenario is qualitatively changed from the discrete situation: for the case of the propagation of a plane wave with a small impurity in a lattice, we have shown that the spectrum of the emitted phonons is different, giving a quite different criterion for the superfluidity.

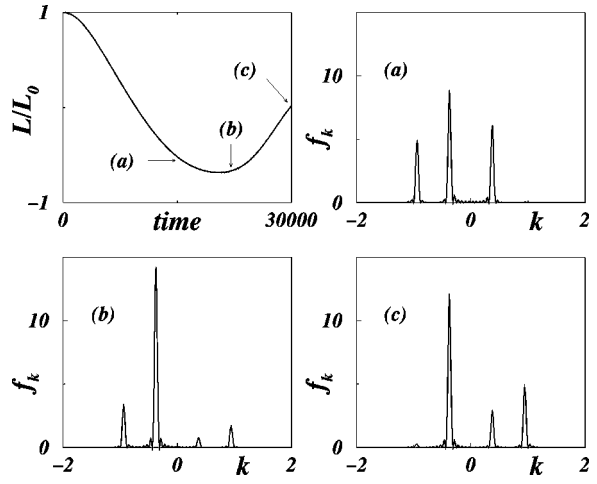

FIG. 19. Normalized angular momentum and Fourier transform f_k at times marked, respectively, as (a)–(c) with two initial waves: $\psi_n(0)=\sqrt{A}e^{ik_1 n}+\sqrt{C}e^{ik_2 n}$, with $A=0.8$ and $C=0.2$. Other parameters are $\epsilon=0.01$, $N=100$, $l_1=6$, $l_2=15$, and $\Lambda=2\epsilon/N$.

To recover the CNLS equation (in an annular geometry) from DNLS (4), we write

$$\Lambda=\frac{2mg_0}{\hbar^2 N},$$

$$\epsilon_n=\frac{V_n mL^2}{\hbar N^2},$$

and

$$t=\frac{mL^2}{\hbar N^2\tau},$$

with $V_n\equiv V(x=x_n)$ the defect potential in x_n, L the length of the annulus, and τ the dimensionless time entering in Eq. (4). The CNLS is then obtained in the limit $N\to\infty$. In particular, the critical value for the pendulum oscillations, Eq. (17), becomes

$$\Lambda_c=V_n mL^2/\hbar N^3\to 0. \tag{41}$$

Therefore, approaching the continuous limit, the DNLS pendulum regime collapses to a (strongly) self-trapped state. This prevents the emission of phonons with opposite momenta with respect to the incident wave, whose energy will eventually be dissipated on a much longer time scale, according to the Landau argument.

IV. CONCLUSIONS

In this paper we have studied the dynamical properties of the DNLS with periodic boundary conditions (annular geometry) in the presence of defects. We showed that in the case of a random distribution of defects, a traveling plane wave with initial wave vector k splits in momentum space into two waves with $\pm k$. This allows for a two-mode ansatz in the Fourier space, which maps the dynamics onto an effective nonrigid (with momentum dependent length) pendulum Hamiltonian. This Hamiltonian has a very rich dynamical phase portrait. For instance, the oscillations of the pendulum around $\phi=0$ correspond to states with a vanishing time average of the angular momentum: the initial traveling wave is

completely reflected and refocused. Above a critical value of nonlinearity (not depending on the wave vector k), the initial angular kinetic energy of the pendulum exceeds the energy needed to arrive at the top ($\phi=\pi$), and a steady self-sustained pendulum rotation occurs, with nonzero angular momentum and a closed-loop trajectory around the pendulum support. This corresponds to a superfluid state, in which the plane wave travels coherently through the randomly distributed defects. This scenario is qualitatively different in the continuum case: a well-known argument suggested by Landau (see Ref. [20]) implies that a finite nonlinearity allows a superfluid regime when the traveling speed is smaller than the sound velocity (for weak perturbations). The nonlinearity provides an effective energy barrier against the creation of elementary excitations with momenta $k+q,k-q$ (with q being arbitrarily small), which would dissipate the energy of the incident wave having momentum k. Therefore, unlike the discrete case, the superfluid propagation of a wave depends on its momentum k.

In conclusion, the two-mode ansatz (7) is valid for an arbitrary distribution of defects in a wide range of values of parameters, and gives an analytically solvable Hamiltonian model, Eq. (25), which successfully reproduces the full numerical solutions of the discrete nonlinear Schrödinger equation. A significant subject of future work will be devoted to the extension of this model to calculate the transmission coefficients in an open, infinite chain with defects.

[1] A.C. Scott, *Nonlinear Science: Emergence and Dynamics of Coherent Structures* (Oxford University Press, New York, 1999).

[2] S. Flach and C.R. Willis, Phys. Rep. **295**, 182 (1998).

[3] N. Mott, *Conduction in Non-Crystalline Materials* (Oxford University Press, New York, 1987).

[4] M. Peyrard *et al.*, Physica D **68**, 104 (1993).

[5] A. Trombettoni, A. Smerzi, and A.R. Bishop, Phys. Rev. Lett. **88**, 173902 (2002).

[6] T.V. Ramakrishnan, in *Chance and Matter*, Proceedings of the Les Houches Summer School, Session XLVI, edited by J. Souletie, J. Vannimenus, and R. Stora (North-Holland, Amsterdam, 1987), p. 213.

[7] S.P. Novikov, L.P. Pitaevskii, V.E. Zakharov, and S.V. Manakov, *Theory of Solitons: The Inverse Scattering Method* (Consultants Bureau, New York, 1984).

[8] M.J. Ablowitz and P.A. Clarkson, *Solitons, Nonlinear Evolution Equations and Inverse Scattering* (Cambridge University Press, Cambridge, England, 1991).

[9] B.P. Anderson and M.A. Kasevich, Science **282**, 1686 (1998).

[10] F.S. Cataliotti *et al.*, Science **293**, 843 (2001).

[11] O. Morsch, J.H. Müller, M. Cristiani, D. Ciampini, and E. Arimondo, Phys. Rev. Lett. **87**, 140402 (2001).

[12] H.S. Eisenberg *et al.*, Phys. Rev. Lett. **81**, 3383 (1998).

[13] R. Morandotti *et al.*, Phys. Rev. Lett. **83**, 2726 (1999).

[14] R. Morandotti *et al.*, Phys. Rev. Lett. **83**, 4756 (1999).

[15] F. Dalfovo, S. Giorgini, L.P. Pitaevskii, and S. Stringari, Rev. Mod. Phys. **71**, 463 (1999).

[16] A. Trombettoni and A. Smerzi, Phys. Rev. Lett. **86**, 2353 (2001).

[17] D. Hennig and G.P. Tsironis, Phys. Rep. **307**, 334 (1999), and references therein.

[18] Yu.S. Kivshar and M. Peyrard, Phys. Rev. A **46**, 3198 (1992).

[19] A. Smerzi, A. Trombettoni, P.G. Kevrekidis, and A.R. Bishop, Phys. Rev. Lett. **89**, 170402 (2002).

[20] A.J. Leggett, Rev. Mod. Phys. **73**, 307 (2001).

[21] A. Smerzi, S. Fantoni, S. Giovanazzi, and S.R. Shenoy, Phys. Rev. Lett. **79**, 4950 (1997).

[22] R. Scharf and A.R. Bishop, Phys. Rev. A **43**, 6535 (1991); Phys. Rev. E **47**, 1375 (1993).

[23] M.I. Molina, Phys. Rev. B **58**, 12 547 (1998).

[24] V.M. Kenkre and D.K. Campbell, Phys. Rev. B **34**, 4959 (1986).

[25] S. Raghavan, A. Smerzi, S. Fantoni, and S.R. Shenoy, Phys. Rev. A **59**, 620 (1999).

[26] R.E. Graham, D.E. Knuth, and O. Patashnik, *Concrete Mathematics: A Foundation for Computer Science* (Addison-Wesley, Reading, MA, 1989).